

Cosmic String Lens Phenomenology: Model of Poisson Energy Distribution

Francis Bernardeau¹ and Jean-Philippe Uzan^{2,3}

(1) *Service de Physique Théorique, CE de Saclay
F-91191 Gif-sur-Yvette Cedex (France).*

(2) *Laboratoire de Physique Théorique, UMR-8627 du CNRS, université Paris XI,
bâtiment 210, F-91405 Orsay cedex (France)*

(3) *Département de Physique Théorique, Université de Genève,
24 quai E. Ansermet, CH-1211 Geneva 4 (Switzerland)*

(October 27, 2018)

We present a novel approach for investigating lens phenomenology of cosmic strings in order to elaborate detection strategies in galaxy deep field images. To account for the complexity of the projected energy distribution of string networks we assume their lens effects to be similar to those of a straight string carrying a *random* lineic energy distribution. In such a model we show that, unlike the case of uniform strings, critical phenomena naturally appear. We explore the properties of the critical lines and caustics. In particular, assuming that the energy coherence length along the string is much smaller than the observation scale, we succeeded in computing the total length of critical lines per unit string length and found it to be $4/\sqrt{3} \mathbf{E}(3/4)$. The length of the associated caustic lines can also be computed to be $16/(\pi\sqrt{3}) \mathbf{E}(3/4)$. The picture we obtain here for the phenomenology of cosmic string detection is clearly at variance with common lore.

PACS numbers: 98.62.Sb, 98.80.Es, 98.80.Cq, 98.80.Hw

Preprint numbers: LPT-ORSAY 00/34, UGVA-DPT 00/03-1075, SPhT-Saclay 00/052

I. INTRODUCTION

Although the current results on large-scale structure formation favor models with initial adiabatic scalar perturbation [1], the formation of cosmic strings is general enough to merit further investigations [2]. It is in particular not excluded that strings may form after an inflationary phase [3]. We are interested here in the phenomenological aspects of cosmic strings for lens distortion effects whereas most of the previous investigations have been focused on string detection from multiple quasar images [4,5] or Cosmic Microwave Background fluctuations [6]. With the advance of new generation of large CCD cameras the best direct evidence for cosmic string relics is however likely to be obtained from distortion effects they induce on background objects such as galaxies.

In a companion paper we insist on the generic properties expected for cosmic strings as far as lens effects are concerned: string lens effects are equivalent to those induced by a lineic energy distribution. This effective energy distribution should obviously take into account the lens energy density, its tension, as well as kinetic energy that might result from rapid movements or energy currents along the string [7].

The explicit computation of string induced lens effects has been done in various cases, for long strings [2], circular loops in plane transverse to the line of sight [8], or small loops with a multipole expansion approach [4]. However, much more complex situations have been explored so far with numerical experiments only [9]. In particular the study presented in [10] suggests a quite different lens phenomenology for the images of background galaxies but lacks analytical insights. Having in mind such phenomenological effects, we try in this paper to

get more quantitative results by introducing a simplified description of strings. In Sect. II we present the model of “Poisson” energy distribution we use. In Sect. III general phenomenological properties observed in such a model are presented. Sect. IV is devoted to more precise calculations on the properties of the critical lines and caustics for such a model of strings and finally we evoke observational aspects.

II. STRING MODEL

A. General formalism

In general lens effects are encoded in an amplification matrix, \mathcal{A} , which describes the way the angular positions in the image plane are transformed to those in the source plane (see [11] for a comprehensive description of lens physics). It is usually written in terms of the convergence field κ and the shear field (γ_1, γ_2) ,

$$\mathcal{A} = \begin{pmatrix} 1 - \kappa - \gamma_1 & -\gamma_2 \\ -\gamma_2 & 1 - \kappa + \gamma_1 \end{pmatrix}, \quad (1)$$

that are directly related to the projected energy density. The remarkable property for lens effects are obtained when one of the eigenvalues of \mathcal{A} is crossing or getting close to zero. The difficulty however is that these features are neither local nor linear in the energy density and location of the string. The fact that the projected density is likely to fluctuate substantially, because of local velocities, wiggles, longitudinal motions etc..., has somehow to be incorporated in the description.

In case of cosmic strings, the elements of the deformation matrix can be derived the effective projected potential $\varphi(x, y)$ which can formally be written in terms of the angular positions (x, y) (e.g. Eq. (37) of [12]) as,

$$\varphi(x, y) = 4G \frac{D_{\text{LS}}}{D_{\text{OS}}} \int ds \mu[x_{\text{str.}}(s), y_{\text{str.}}(s)] \times \log \left([x - x_{\text{str.}}(s)]^2 + [y - y_{\text{str.}}(s)]^2 \right)^{1/2} \quad (2)$$

where $(x_{\text{str.}}(s), y_{\text{str.}}(s))$ are the angular string coordinates for the angular curvilinear position s , $\mu(x_{\text{str.}}(s), y_{\text{str.}}(s))$ is the projected energy density at those positions, G is the Newton constant and $D_{\text{LS}}/D_{\text{OS}}$ is the ratio of the angular distance between the string and the source-plane to the one between the observer and the source plane in the thin lens* approximation [12]. The projected energy density is a combination of the projected T_{00} , T_{0z} and T_{zz} components of the stress-energy tensor of the string if the line-of-sight is along the z direction. The displacement field is then given by

$$\xi_i = -\partial_i \varphi(x, y) \quad (3)$$

and the elements of the deformation matrix can be written as,

$$\begin{aligned} \gamma_1 &= (\partial_x^2 - \partial_y^2) \varphi(x, y), \\ \gamma_2 &= 2 \partial_x \partial_y \varphi(x, y), \end{aligned} \quad (4)$$

the local convergence being zero except on the string itself.

B. The Poisson string model

It seems very difficult to take into account all the features that must be included: the string are far from being straight lines with uniform energy distribution [9]. We choose to describe the energy fluctuation in a simple manner, assuming that the string follows a straight line, but with local energy fluctuations. This fluctuations are assumed to account for the various changes of shape, density of the strings, for possible non-standard equation of states, or for the existence of currents along the string. We therefore assume the string to be straight along the y direction,

$$x_{\text{str.}}(s) = 0, \quad y_{\text{str.}}(s) = s \quad (6)$$

and $\mu(s)$ to be a random field. Note that it does not mean however that the string is actually orthogonal to the line-of-sight. It simply means that the string (or rather the

section of string we are interested in) appears roughly straight on the sky. To specify our model we still need to explicit the statistical properties of the μ field. In general the results are going to depend on the chosen global statistical properties of μ and not only on its 2-point function for instance. In particular one question to ask is whether there is a finite correlation length along the string or not. Let us assume that the string can be described by the following properties,

$$\langle \mu(s) \rangle = \mu_0 \quad (7)$$

$$\langle \mu(s_1) \mu(s_2) \rangle_c = c_2 \mu_0^2 \exp \left[-\frac{|s_1 - s_2|}{s_0} \right] \quad (8)$$

$$\begin{aligned} \langle \mu(s_1) \dots \mu(s_p) \rangle_c &= c_p \mu_0^p \times \\ &\exp \left[-\frac{\max\{s_p\} - \min\{s_p\}}{s_0} \right] \end{aligned} \quad (9)$$

so that $\mu(s)$ has a finite coherence length, s_0 , and $\mu(s)$ is essentially uniform with typical value μ_0 at scales smaller than s_0 . The statistical properties of the displacement field or of the elements of the amplification matrix are then described by the ones of μ . For instance,

$$\begin{aligned} \langle \gamma_i^p(x) \rangle_c &= c_p G^p \frac{D_{\text{LS}}^p}{D_{\text{OS}}^p} \mu_0^p \times \\ &\int_{-\infty}^{+\infty} ds_1 \dots \int_{-\infty}^{+\infty} ds_p G_i(x, s_1) \dots G_i(x, s_p) \times \\ &\exp \left[-\frac{\max\{s_p\} - \min\{s_p\}}{s_0} \right], \end{aligned} \quad (10)$$

with

$$G_1(x, y) = 4 \frac{y^2 - x^2}{(y^2 + x^2)^2}, \quad (11)$$

$$G_2(x, y) = -8 \frac{xy}{(y^2 + x^2)^2}. \quad (12)$$

The general expressions of these integrals are complicated, but they can be computed at leading order is s_0/x . First of all we can notice that

$$\langle \gamma_1 \rangle = \langle \gamma_2 \rangle = 0. \quad (13)$$

At leading order in s_0/x the computation of the results can be obtained by an expansion of $G_i(x, s_j)$ with respect to s_j in the vicinity of s_1 (for instance) as

$$G_i(x, s_j) = \sum_p \frac{(s_j - s_1)^p}{p!} \frac{\partial^p G_i}{\partial s^p}(x, s_1). \quad (14)$$

It leads to

$$\begin{aligned} \langle \gamma_i^2 \rangle &\approx 8c_2 G^2 \frac{D_{\text{LS}}^2}{D_{\text{OS}}^2} \mu_0^2 \int_{-\infty}^{+\infty} ds_1 G_i(x, s_1) \times \\ &\int_0^{+\infty} ds_2 G_i(x, s_1 + s_2) \exp(-s_2/s_0) \end{aligned} \quad (15)$$

$$\approx 8c_2 G^2 \frac{D_{\text{LS}}^2}{D_{\text{OS}}^2} \mu_0^2 s_0 \int_{-\infty}^{+\infty} ds G_i^2(x, s). \quad (16)$$

*The thin lens approximation is appropriate if one is interested in only a fraction of a string spanning at most a few degrees on the sky. This would not be appropriate for apparent string crossings for instance.

A similar computation can be performed for the third cumulant,

$$\langle \gamma_i^3 \rangle = 48 c_3 G^3 \frac{D_{\text{LS}}^3}{D_{\text{OS}}^3} \mu_0^3 s_0^2 \int_{-\infty}^{+\infty} ds G_i^3(x, s). \quad (17)$$

One can further notice that for parity reasons $\langle \gamma_2^3 \rangle = 0$. For the first component of the shear we however have

$$\langle \gamma_1^2 \rangle = 8 c_2 s_0 G^2 \frac{D_{\text{LS}}^2}{D_{\text{OS}}^2} \mu_0^2 \frac{4\pi}{x^3}, \quad (18)$$

$$\langle \gamma_1^3 \rangle = -48 c_3 s_0^2 G^3 \frac{D_{\text{LS}}^3}{D_{\text{OS}}^3} \mu_0^3 \frac{8\pi}{x^5}. \quad (19)$$

One can notice that the dimensionless skewness $\langle \gamma_1^3 \rangle / \langle \gamma_1^2 \rangle^{3/2}$ is given by

$$\frac{\langle \gamma_1^3 \rangle}{\langle \gamma_1^2 \rangle^{3/2}} = -\frac{6}{\sqrt{8\pi}} \left(\frac{s_0}{x} \right)^{1/2} \frac{c_3}{c_2^{3/2}}. \quad (20)$$

The ratio $c_3/c_2^{3/2}$ being a priori finite (and surely the one-point probability distribution function of μ has no reason to obey Gaussian statistics), it implies that the reduced skewness vanishes at distance much larger than the correlation length s_0 from the string. This is a natural expectation since at finite distance and for $s_0 \rightarrow 0$ such quantities as the shear are obtained as sums of infinite number of sources. So, very generically, whatever may be the statistical properties of μ , we expect that locally, all quantities follow Gaussian statistics as soon as $x \gg s_0$.

In the following we will thus assume to be in this regime, that is we assume that the energy distribution along the string has a vanishing coherence length. In this case the exponential factor can be replaced by a Dirac delta function so that the 2-point correlation function of μ can be written,

$$\langle \mu(s_1) \mu(s_2) \rangle = 2 c_2 s_0 \mu_0^2 \delta_{\text{Dirac}}(s_1 - s_2) \quad (21)$$

and the other correlation functions are then not relevant for the description of the distortion properties. (It does not mean that the probability distribution function of μ is assumed to be Gaussian distributed!). Obviously, this result does not depend on the details of the small scale correlation properties of μ . One can see that in this limit only one extra parameter is required to describe μ , that is $c_2 s_0$. Since it is not a priori possible to distinguish between the coherence length s_0 and c_2 , in the following we use Eq. (21) assuming that $c_2 = 1/2$.

Together with Eq. (6) we call this model of strings, the *Poisson string model*. We are aware of the dramatic simplifications we have adopted to describe the outcome of an a priori very complicated physics. Still we think that some of the basic properties of lens phenomenology can be captured by such a model in a much more realistic way than a simple straight string with a uniform distribution.

III. ELEMENTARY PHENOMENOLOGY OF "POISSON STRING"

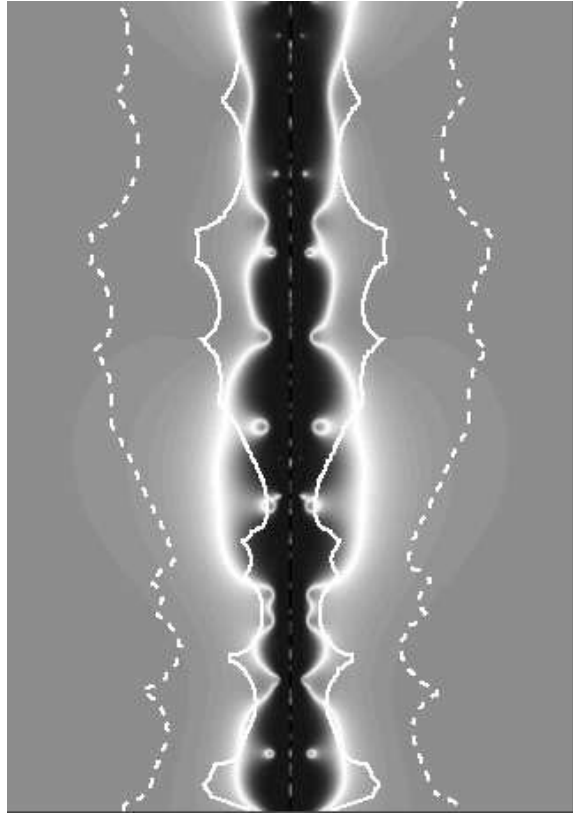


FIG. 1. Numerical experiment showing the amplification map, i.e. $1/\det(\mathcal{A})$, of a “Poisson string”. The brightest pixels correspond to infinite magnification: they form the critical lines. The darkest pixels correspond to a magnification close to zero. The solid lines correspond to the caustics, positions of the critical lines in the source plane. The external dashed lines are the counter images of the critical lines.

On Fig. 1 we depict an example of numerical implementation of such a cosmic string, showing various features associated with this lens system. It is obviously beyond the scope of this article to present the general theory of gravitational lenses (see [13]). The aim of this section is to give some hints on the expected phenomena encountered for such a model of energy distribution.

The grey levels show the variation of amplification given by the determinant of \mathcal{A}^{-1} . Along the brightest areas the amplification is infinite; these locations form the critical lines. This is where the most dramatic lens effects could be detected: giant arcs, merging of images... Note that such lines simply do not exist for strings with uniform density! The critical lines are mainly made of two long lines running along the string without crossing it. This latter property is due to the fact that whatever the local value of μ the displacement field has always an infinite gradient at the string position. This point will be quantified more precisely in the next section.

Such a system of critical lines is associated with caustic lines in the source plane. These caustic lines are shown on Fig. 1 as thick solid lines: the left one for instance is obtained by applying the displacement field to the right side long critical line. If a background object happens to lie on this line, it will appear as a highly deformed object (with formally infinite magnification) on the image plane. The caustic lines are also directly related to the possibility of having multiple image of background objects. Each time one is crossing the caustic lines the number of associated images is changed by 2: at large distance the number of image is one; after one crossing it has 3 (in other words if an object is located in between the two caustic lines, it has 3 images), after 2 crossings it has either 1 again or 5 (this is the case for the caustic lines associated to the inner critical lines), etc...

Thus, in general, on the image plane the critical lines are betrayed by dramatic lens effects such as merging of two images of background objects. It is then worth noting that we are here generically in a regime of 3 images in the vicinity of the string (except in rare cases where it can be 5) instead of 2 as for a strictly uniform string. The dashed lines show the locations of the counter images of the critical lines. It delimits the region, in the image plane, within which multiple images can be found. It can be noted however that the amplification rapidly decreases in the vicinity of the string, so that central images (i.e. the ones situated in between the two infinite critical lines) are expected to be strongly de-amplified, except when they are close to one of the critical lines.

Moreover, the examination of Fig. 4 shows that numerous small images generically appear along the string. The presence of these images are due to the fluctuating small scale structure of the string. They are associated with an infinite number of critical lines (and caustics) near the string, that are only partially exhibited on Fig. 1 due to the finite resolution of our simulation. In a realistic string these images would appear down to scales corresponding to the coherence scale s_0 . One aim of the next section is again to quantify more precisely this aspect.

We have checked that, in the limit of the resolution of this simulation, the global feature we see here do not depend on the shape of the one-point probability distribution function of μ neither on the actual resolution.

IV. STATISTICAL PROPERTIES

The aim of this section is to quantify some aspects of the results described in the previous part. Indeed, in general systems of critical lines depend non-trivially on the lens strength and also on the optical bench configuration. So, at this point, it is not clear how typical is the plot presented on Fig. 1, and whether it depends or not on the parameter choice. Other aspects that may be difficult to grasp with a simple numerical experiment are

the mathematical properties of the critical lines. Since the strings has an infinite number of substructures (when the coherence length is assumed to vanish) the properties of the critical and caustic lines may not be numerically stable. In particular there seem to be a large number of small critical lines close to the string. So we do not know a priori whether those lines form a fractal like structure, or whether their total length is finite.

In the following we want in particular to locate the position of the critical lines, compute their average length (per unit string length) as well as the length of their counterparts in the source plane, the caustic lines. And quite surprisingly, what in general would be an impossible task (because critical lines form complex patterns that depend nonlinearly and nonlocally on the energy distribution) turns out to be computable to a large extent for this model.

The calculations are primarily based on the fact that all local quantities obey Gaussian statistics and can thus be entirely described by their second moments. This property is valid because we assume to be in a regime of an infinitely small coherence length on the string. This would not have been the case otherwise, and not only should the correlation effects of μ along the string be taken into account but also the fact that $\mu(s)$ itself is not a priori Gaussian distributed.

The calculations of the moments of the displacement, the shear components and the shear gradients are the required ingredients and are given first.

A. Correlation matrices

1. Displacement field

Not surprisingly we can check that,

$$\langle \xi_1(x) \rangle = -\xi_0 \text{sign}(x) \quad (22)$$

$$\langle \xi_2(x) \rangle = 0 \quad (23)$$

where

$$\xi_0 \equiv 4\pi G \frac{D_{\text{LS}}}{D_{\text{OS}}} \mu_0, \quad (24)$$

which corresponds to the case of a uniform cosmic string. We introduce the angular variable ξ_0 that defines the average energy scale of the string. The second moment of the displacement field is given by,

$$\langle \xi_i(x) \xi_j(x) \rangle = \frac{8\pi}{x} s_0 \mu_0^2 \delta_{ij} = \frac{1}{2\pi x} s_0 \xi_0^2 \delta_{ij}. \quad (25)$$

One can note that the displacement fluctuations have the same amplitude in directions along the string and perpendicular to the string (we have no convincing physical interpretation for that). A consequence of these results is that angular pair separations is no more fixed, (and given by $2\xi_0$); they may fluctuate along the string, and

the amplitude of the fluctuations is all the more large that the images are close to the string. The image pairs may also not be strictly orthogonal to the string direction. The amplitude of these fluctuations depend on the dimensionless ratio s_0/ξ_0 . The larger it is, the larger the relative fluctuations are.

Such effects can be observed on Figs. 4, where pairs can be clearly identified, but distances and orientations indeed fluctuate from pair to pair.

2. Amplification matrix

As we already stressed, the main novel effect compared to a uniform straight string is the emergence of complex distortion features. The latter are related to the value of the local shear. For a uniform string the shear components are always zero. A reminder of this property is given by the average values of the elements of the amplification matrix that all vanish.

The shear components are explicitly given by

$$\gamma_1 = 8G \frac{D_{\text{LS}}}{D_{\text{OS}}} \int ds \mu(s) \frac{(y-s)^2 - x^2}{((y-s)^2 + x^2)^2}, \quad (26)$$

$$\gamma_2 = -16G \frac{D_{\text{LS}}}{D_{\text{OS}}} \int ds \mu(s) \frac{(y-s)x}{((y-s)^2 + x^2)^2}. \quad (27)$$

Their second moments can be calculated[†]. They depend on the distance to the string and are given by

$$\langle \gamma_i(x) \gamma_j(x) \rangle = \frac{1}{\pi x^3} s_0 \xi_0^2 \delta_{ij}. \quad (28)$$

For completeness we can also compute the cross-correlation terms,

$$\langle \gamma_i(x) \xi_j(x) \rangle = -\frac{1}{4\pi x^2} s_0 \xi_0^2 \delta_{ij}, \quad (29)$$

with the displacement field. These results allow us to gain some insights into this system. For instance one can compute that the local shear distribution function. It is given by,

$$\mathcal{P}(\gamma) d\gamma = \exp \left[-\frac{\gamma^2}{2\sigma_\gamma^2} \right] \frac{\gamma d\gamma}{\sigma_\gamma^2} \quad (30)$$

where

$$\sigma_\gamma^2 = \langle \gamma^2 \rangle = \langle \gamma_1^2 \rangle. \quad (31)$$

Since the local convergence vanishes, the local amplification $\mu = 1/\det \mathcal{A}$ is given by

$$\mu = \frac{1}{1 - \gamma^2}, \quad (32)$$

and the critical lines are the locations where $\gamma = 1$. From the relation (30), we can compute the probability that a point at a given location is within the critical zone ($\gamma > 1$) or out ($\gamma < 1$). This probability is given by,

$$\begin{aligned} \mathcal{P}_{\text{crit.}}(x) &= \int_1^\infty \mathcal{P}(\gamma) d\gamma = \exp \left[-\frac{1}{2\sigma_\gamma^2(x)} \right] \\ &= \exp \left[-\frac{\pi x^3}{2s_0 \xi_0^2} \right]. \end{aligned} \quad (33)$$

This probability has a very simple shape. It reaches unity nearby the string. This expresses the fact that the string itself is always in the critical region: no critical lines can actually cross the string, and there must always exist two infinite critical lines running on each side of the string. The situation observed on Fig. 1 is thus completely generic in this respect.

This expression also indicates the behavior of typical critical line distance to the string. It must scale somehow as $(s_0 \xi_0^2)^{1/3}$ since this is the only distance that intervenes in Eq. (33). The exact calculation of such a quantity cannot however be obtained from the mere distribution of the shear. The number of intersection points between the critical lines and any horizontal lines for instance is also not contained in the probability. Somehow the spatial correlations of the shear have to be taken into account. We will see in the following that the statistical properties of the shear gradients allow the computation of such quantities.

3. Shear gradients

They are a priori four different shear gradient components. However, since the local convergence is zero, there are simple relations that relate these components together,

$$\partial_x \gamma_2 = \partial_y \gamma_1, \quad (34)$$

$$\partial_y \gamma_2 = -\partial_x \gamma_1, \quad (35)$$

so that only two quantities have to be considered. We can furthermore define a pseudo-vector $\vec{\delta}$ as $\vec{\delta} \equiv (\partial_x \gamma_1, \partial_y \gamma_1)$. The calculations of its statistical properties can be done in a similar way as previously, and one gets

$$\langle \delta_i(x) \delta_j(x) \rangle = \frac{3}{\pi x^5} s_0 \xi_0^2 \delta_{ij}, \quad (36)$$

$$\langle \gamma_i(x) \delta_j(x) \rangle = -\frac{3}{2\pi x^4} s_0 \xi_0^2 \delta_{ij}, \quad (37)$$

from which we deduce that the correlation coefficient r with the shear field is given by

[†]It is actually possible to also compute analytically the two-point correlation functions, $\langle \gamma_i(x, y) \gamma_j(x', y') \rangle$, but it has no use in the following.

$$\begin{aligned}
r &\equiv \frac{\langle \gamma_1 \delta_1 \rangle}{\sqrt{\langle \delta_1^2 \rangle \langle \gamma_1^2 \rangle}} = \frac{\langle \gamma_2 \delta_2 \rangle}{\sqrt{\langle \delta_2^2 \rangle \langle \gamma_2^2 \rangle}} \\
&= -\frac{\sqrt{3}}{2} \approx -0.86.
\end{aligned} \tag{38}$$

As a result we can explicitly write the joint probability distribution of the local shear and shear gradients,

$$\begin{aligned}
&\mathcal{P}(\vec{\gamma}, \vec{\delta}) d^2 \vec{\gamma} d^2 \vec{\delta} = \\
&\exp \left[-\frac{1}{2(1-r^2)} \left(\frac{\gamma^2}{\sigma_\gamma^2} + \frac{\delta^2}{\sigma_\delta^2} - \frac{2r \vec{\gamma} \cdot \vec{\delta}}{\sigma_\gamma \sigma_\delta} \right) \right] \times \\
&\frac{1}{(1-r^2)(2\pi)^2} \frac{d^2 \vec{\gamma} d^2 \vec{\delta}}{\sigma_\gamma^2 \sigma_\delta^2},
\end{aligned} \tag{39}$$

where r is given by (38), σ_γ is defined in Eq. (31) and σ_δ is given by $\sigma_\delta^2 = \langle \delta_1^2 \rangle = \langle \delta_2^2 \rangle$.

B. Properties of the critical lines

1. Where are the critical lines?

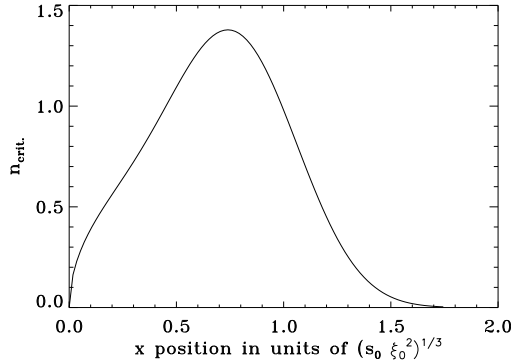


FIG. 2. Shape of the function $\bar{n}_{\text{crit.}}(x)$ as a function of the distance from the string in units of $(s_0 \xi_0^2)^{1/3}$.

As mentioned previously we are now in position to address issues related to the critical and caustic lines. First thing that can be considered is the number density, $\bar{n}_{\text{crit.}}(x)$, of intersection point between the critical line and any horizontal axis. This function will allow us to compute not only the typical number of such intersection points but also the average distance between the critical lines and the string, and its fluctuations. The method we introduce here will also be employed in the next paragraph to derive the total length of the critical lines.

If x_i denote the locations where $\det(\mathcal{A}) = 0$ (which is equivalent to $\gamma = 1$ when $\kappa = 0$) on a given horizontal axis, the local number density of intersecting points is

$$n_{\text{crit.}}(x) = \sum_i \delta_{\text{Dirac}}(x - x_i), \tag{40}$$

where each x_i is an implicit function of the random variables $\mu(s)$. Such a quantity is actually a random quantity that depends in particular on the y position. But what we really want is the average number density of these points, that would be measured as a geometrical average over y position,

$$\bar{n}_{\text{crit.}}(x) = \frac{1}{L} \int_0^L dy n_{\text{crit.}}(x), \tag{41}$$

in the limit of a large L . If we assume this system to be ergodic, then the geometrical average of Eq. (41) can be replaced by an ensemble average over the positions x_i (that are random quantities depending on the variables, $\vec{\gamma}$, $\vec{\delta}$, etc...) as,

$$\bar{n}_{\text{crit.}}(x) = \int \mathcal{P}(\vec{\gamma}, \vec{\delta}, \dots) d^2 \vec{\gamma} d^2 \vec{\delta} \dots \sum_i \delta_{\text{Dirac}}(x - x_i). \tag{42}$$

To perform such an average, one needs to make a change of variable from x_i to local parameters $\vec{\gamma}$ and $\vec{\delta}$. This is possible since we need to do this change of variable only in the vicinity of x_i (we follow here the same line of computation as what has been done in 3D or 2D Gaussian fields for computations of number density of maxima [14]). The constraint $(x - x_i) = 0$ can then be replaced by a constraint on the random variables $\vec{\gamma}$ and $\vec{\delta}$. Since at first order in $(x - x_i)$,

$$\gamma(x) \approx 1 + (x - x_i) \partial_x \gamma(x_i) \tag{43}$$

we obtain that

$$\bar{n}_{\text{crit.}}(x) = \int \mathcal{P}(\vec{\gamma}, \vec{\delta}) d^2 \vec{\gamma} d^2 \vec{\delta} \delta_{\text{Dirac}}(\gamma - 1) |\partial_x \gamma|, \tag{44}$$

with

$$\partial_x \gamma = \frac{1}{2} (\gamma_1 \delta_1 + \gamma_2 \delta_2) = \frac{1}{2} \vec{\gamma} \cdot \vec{\delta}. \tag{45}$$

The integral (44) can then be easily computed explicitly using the expression (39). It leads to

$$\begin{aligned}
\bar{n}_{\text{crit.}}(x) &= \sqrt{\frac{3x}{2}} e^{-2\pi x^3} + \\
&\frac{3}{2} \pi x^2 \text{Erf}\left(\sqrt{\frac{3\pi}{2}} x^{\frac{3}{2}}\right) e^{-\frac{\pi x^3}{2}},
\end{aligned} \tag{46}$$

when x is taken in units of $(s_0 \xi_0^2)^{1/3}$. As shown on Fig. 2 where we have depicted $\bar{n}_{\text{crit.}}(x)$, the intersections mostly take place at a distance of about $0.75 (s_0 \xi_0^2)^{1/3}$. The average number of intersection points (on one side of string) is then

$$\bar{n} = \int_0^{+\infty} dx n_{\text{crit.}}(x) = \frac{2}{\sqrt{3}} \approx 1.155. \tag{47}$$

The number of intersection points being an odd number, it means that the critical line crosses one horizontal line more than once in at most 7% of the cases. It supports the fact that we are dominated by the two long critical lines located on each side of the string. In rare cases, inner critical lines can give rise to complex multiple image systems.

The typical distance of the critical lines to the string can also be computed. It is given by

$$d_{\text{crit.}} = \frac{\int_0^{+\infty} dx x \bar{n}_{\text{crit.}}(x)}{\int_0^{+\infty} dx \bar{n}_{\text{crit.}}(x)} \approx 0.70 (s_0 \xi_0^2)^{1/3} \quad (48)$$

whereas the scatter of this distance is about

$$\Delta d_{\text{crit.}} = 0.31 (s_0 \xi_0^2)^{1/3}. \quad (49)$$

One recovers the scaling behavior suggested in previous paragraph. Remarkably the average distance and the scatter of the distance follow the same scaling law. It suggests that the critical line system is somehow universal, in the sense that it does not depend on the dimensionless ratio s_0/ξ_0 . This idea is further supported in the next paragraph where we compute the total length of the critical lines.

2. Length of the critical lines

The length of the critical lines (per unit string length L) is a priori given by

$$L_{\text{crit.}} = 2 \int_0^\infty dx \int_0^L dy \delta_{\text{Dirac}}(x-x_c, y-y_c) \quad (50)$$

where (x_c, y_c) describes the running position of the critical lines in the (x, y) plane and the factor 2 accounts to the fact that we take into account both side of the string. To complete this calculation one can perform a change of variables from (x, y) to (u_c, v_c) where u_c and v_c are the coordinates of a point in a basis given by (\vec{n}, \vec{t}) , normal and tangential vectors to the critical line at (x_c, y_c) position. Then the integral (50) reads

$$L_{\text{crit.}} = 2 \int du_c dv_c \delta_{\text{Dirac}}(u_c). \quad (51)$$

As previously the δ_{Dirac} function can be replaced by a constraint on γ . In this case the modulus of the gradient along the x direction is replaced by the one along the \vec{n} direction which is $|\nabla\gamma|$ by construction. Finally one gets, returning to the x and y variables,

$$L_{\text{crit.}} = 2 \int_0^\infty dx \int_0^L dy \int \mathcal{P}(\vec{\gamma}, \vec{\delta}) d^2\vec{\gamma} d^2\vec{\delta} \times |\nabla\gamma| \delta_{\text{Dirac}}(\gamma - 1). \quad (52)$$

This can also be computed straightforwardly by noting that

$$\nabla\gamma = \frac{1}{2} (\gamma_1\delta_1 + \gamma_2\delta_2, \gamma_1\delta_2 - \gamma_2\delta_1) \quad (53)$$

so that

$$|\nabla\gamma| = \gamma\delta. \quad (54)$$

The integral over y is then straightforward and gives a factor L . The integral over δ can be performed without too much difficulty and gives,

$$L_{\text{crit.}} = L 2\sqrt{6} \pi^2 \times \int_0^\infty dx x^{7/2} I_0\left(-\frac{3\pi x^3}{4}\right) \exp\left(-\frac{5\pi x^3}{4}\right) \quad (55)$$

where I_0 is the Bessel function. Finally, using an integral representation of I_0 , one finds

$$L_{\text{crit.}} = \frac{4}{\sqrt{3}} \mathbf{E}\left(\frac{3}{4}\right) L \approx 2.80 L, \quad (56)$$

where \mathbf{E} is the complete elliptic integral. Remarkably this coefficient is independent of the parameter of the model. In particular it does not depend on the dimensionless ratio s_0/ξ_0 . Because this integral is finite, it also proves that the closed critical lines have a finite total length despite the fact that they are in infinite number.

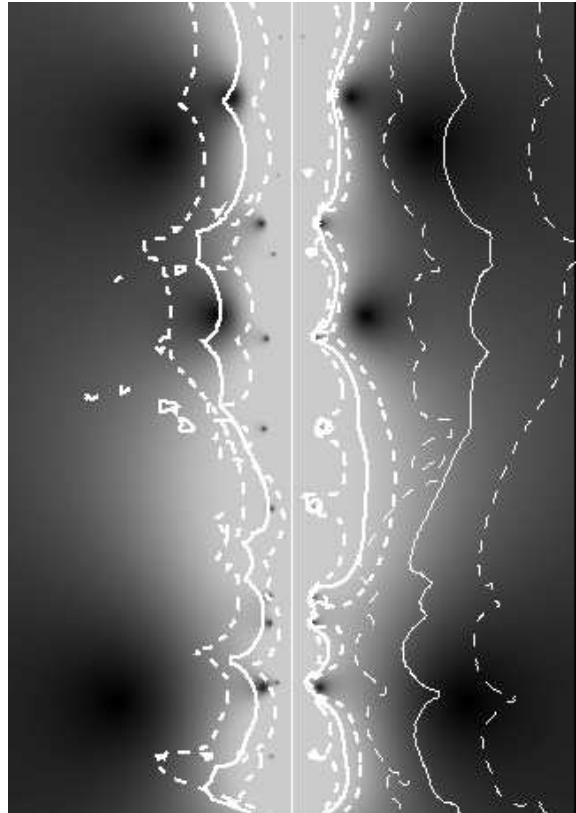


FIG. 3. From the same numerical experiment we show the variation of the location of the critical (right side) and caustic (left side) lines when the source plane is displaced. The grey levels show here the amplitude of the shear field. We see that the critical lines tend to stick around points where γ vanishes (and the points where it happens are independent on the source plane distance). The thin lines show the variation of the position of the counter image of the caustic lines.

C. Properties of the caustic lines

If one wants to detect such a string with distortion effects, the efficiency of such a detection will be directly proportional to the length of the *caustic* lines which are the locations on the source plane where the background objects are significantly distorted.

The calculation of the length of the caustic lines is a priori a much more difficult task since it is related to quantities in the source plane. One can actually circumvent this problem. The idea is that a length element $d\vec{l}_{\text{crit.}}$ on the critical line is going to be transformed in a length element on the caustic line $d\vec{l}_{\text{caus.}}$ according to the amplification matrix linear transformation

$$d\vec{l}_{\text{caus.}} = \mathcal{A} \cdot d\vec{l}_{\text{crit.}} \quad (57)$$

We are interested here only in the change of length $|d\vec{l}_{\text{crit.}}|$ to $|d\vec{l}_{\text{caus.}}|$. It depends locally on the eigenvalues and eigen-directions of \mathcal{A} . On the critical line the eigenvalues of \mathcal{A} are 0 and 2 (one is necessarily 0 by construction, the other is given by the trace of the matrix, that is 2, since $\kappa = 0$ everywhere). As a result we deduce that

$$|d\vec{l}_{\text{caus.}}| = 2|d\vec{l}_{\text{crit.}} \cdot \vec{e}_2| \quad (58)$$

where $d\vec{l}_{\text{crit.}} \cdot \vec{e}_2$ is the component of $d\vec{l}_{\text{crit.}}$ on the eigen-direction associated with the eigenvalue 2. The eigenvector associated with this eigenvalue is

$$\vec{e}_2 = \frac{1}{\sqrt{2(1+\gamma_1)}} \begin{pmatrix} -\gamma_2 \\ 1+\gamma_1 \end{pmatrix}. \quad (59)$$

If we set

$$\vec{\gamma} = \gamma (\cos \psi, \sin \psi) \quad (60)$$

and

$$\nabla \gamma = \gamma \delta (\cos \phi, \sin \phi) \quad (61)$$

we deduce that

$$\frac{|d\vec{l}_{\text{caus.}}|}{|d\vec{l}_{\text{crit.}}|} = \frac{2}{\sqrt{2(1+\gamma_1)}} |\cos(\phi - \psi) + \cos \psi|. \quad (62)$$

The shear field has no preferred direction and thus it is possible to integrate over ψ with a flat distribution to get

$$\frac{|d\vec{l}_{\text{caus.}}|}{|d\vec{l}_{\text{crit.}}|} = \int_{-\pi}^{\pi} \frac{d\psi}{2\pi} \frac{\sqrt{2}}{\sqrt{1+\gamma_1}} |\cos(\phi - \psi) + \cos \psi| = \frac{4}{\pi} \quad (63)$$

(this can be obtained by the change of variable, $\psi = 2t$). Remarkably this result is independent of ϕ so that we directly conclude that

$$L_{\text{caus.}} = \frac{4}{\pi} L_{\text{crit.}} \approx 3.56 L. \quad (64)$$

From an observational point of view we have obtained with this result some insights into the detectability of such a string from large distortion effects. The cross-section of a Poisson string of length L can be estimated to be about $3.6 L$ times typical galaxy sizes, if galaxies are the objects that one uses to reveal the distortion effects.

D. Cusps number density

One could pursue these investigations by computing the number density of cusps along the critical lines, that is points corresponding to the merging of 3 images. These points are characterized by the property that the critical line is locally along the eigenvector associated with the eigenvalue equal to zero. Technically it corresponds to the cases where $|d\vec{l}_{\text{caus.}}|$ vanishes in previous calculations. Since the detailed calculation of such a quantity requires one further derivatives of the shear, we do not present it here. We can however argue from simple scaling arguments that

$$n_{\text{cusps}} \propto (s_0 \xi_0^2)^{-1/3}. \quad (65)$$

E. Scaling laws

Note that for our description to be valid, the typical distance of the critical line to the string, $(s_0 \xi_0^2)^{1/3}$, must be larger than the coherence length along the string s_0 (assuming c_2 to be finite). This is the case when the average displacement ξ_0 is larger than s_0 .

Changing the position of the source plane is equivalent to changing the amplitude of ξ_0 while keeping s_0 constant. It acts indeed as a normalization factor (see Eq. 24). If this amplitude is multiplied by λ , the angular distance of the critical line to the string scales like,

$$d_{\text{crit.}} \propto \lambda^{2/3}. \quad (66)$$

But still the total length of the critical lines remains unchanged. On Fig. 3 we illustrate this effect by changing the amplitude of ξ_0 . We see that the critical lines (thick lines on the right side) are drifting away from the string.

However they tend to get stuck on points where the local shear vanishes (dark patches on the figure) creating invaginations towards the string position. When ξ_0 gets large enough the critical line is disconnected and leaves a small inner closed critical line around $\gamma = 0$ points. This effect can be observed in particular in the central part of the figure. As a result the critical line has larger position fluctuations, but over a larger scale along the string, so that its total length is kept constant. One consequence of this mechanism is that there are locations on the image plane (close to points where $\gamma = 0$) which correspond to quasi-superposition of critical lines from many different source planes. That should make them more likely to be detected.

At the same time the caustic lines are sweeping over the source plane; their distance to the critical line, and to the string, increases like λ , if the typical displacement is larger than $(s_0\xi_0)^{1/3}$. In this case we can also observe that the size of the multiple image region is determined by the displacement amplitude and thus scales like λ (positions of the thin lines on the right side).

V. DISCUSSIONS

This investigation provides a new description of the phenomenological properties of lens physics for cosmic strings. The model of ‘‘Poisson string’’ we present is based on general results which state that the lens effects of string are those obtained from lineic energy density. We think such a model must have captured most of the generic properties expected for string lens phenomenology as the resemblance with the results of numerical experiments (see Fig. 3 of [10]) strongly suggests it. We are however aware that the validity of the description we adopted has not been demonstrated (numerical simulations of string networks anyway lack the necessary resolution for describing correctly the small scale structures of strings). It is clear for instance that the projected position of a string on the sky does not follow a straight line. We have checked that the results we found are not strongly affected if a non-zero curvature radius is introduced, as long as this radius is larger than the other quantities involved in this problem, i.e. ξ_0 and $(s_0\xi_0^2)^{1/3}$.

The results we have obtained suggest novel strategies for detecting strings: multiple images are still present, but images can have undergone significant distortions; small images of background objects can be found in large numbers... The most adapted strategy depends however on the resolution of the imaging apparatus and on the energy scale of the string. On Fig. 4 we show an example of an HST deformed image. In this case the energy scale of the string expressed in units of ξ_0 is similar to the angular scale of a galaxy. For GUT strings, ξ_0 would be of the order of a few arcsecs which is indeed a typical galaxy size in deep surveys. The probability of observing such an event depends obviously on the survey coverage. The

expected angular length of strings to be present within redshift unity has been estimated in [15] and is such that on average one string is expected to cross a 100 deg² survey. But even though such surveys are within reach in the near future, the probability with which one can detect a string (or conversely the rejection one can put on the existence of strings with a given energy scale) still deserves further investigations in particular on the effects of multi source planes (the amplitude of the lens effects depends on the position of the source plane) that may partly blur the searched effects.

-
- [1] N. Turok, U.-L. Pen and U. Seljak, *Phys. Rev.* **D58** (1998) 023506; A. Albrecht, R. A. Battye and J. Robinson *Phys. Rev.* **D59** (1999) 023508; R. Durrer, M. Kunz and A. Melchiorri, *Phys. Rev.* **D59** (1999) 123005; J.-P. Uzan, N. Deruelle and A. Riazuelo, *Proceedings of the XIXth Texas Meeting*, Paris, december 1998, Eds. P. Peter.
 - [2] T.W.B. Kibble, *J. Math. Phys.* **A9** (1976) 1387; A. Vilenkin and P. Shellard, *Cosmic strings and other topological defects*, Cambridge University Press, Cambridge (1994).
 - [3] R. Jeannerot, *Phys. Rev.* **D56**, 6205-6216 (1999); I. Tkachev, S. Khlebnikov, L. Kofman and A. Linde, *Phys. Lett.* **B440**, 262-268 (1998).
 - [4] A. Vilenkin, *Phys. Rev.* **D23** (1981) 852; A. Vilenkin, *Astrophys. J.* **282** (1984) L51; A. Vilenkin, *Nature* **322** (1986) 613; J.R. Gott III, *Astrophys. J.* **288** (1985) 422; C. Hogan and R. Narayan, *Mon. Not. R. astr. Soc.* **211** (1984) 575.
 - [5] E. M. Hu, *Astrophys. J. Lett.* **360** (1990) L7.
 - [6] N. Kaiser and A. Stebbins, *Nature* **276** (1984) 391; F.R. Bouchet, D.P. Bennett and A. Stebbins, *Nature* **335** (1988) 410.
 - [7] J. Garriga and P. Peter, *Class. Quant. Grav.* **11** (1994) 1743.
 - [8] A.A. de Laix and T. Vachaspati, *Phys. Rev.* **D54** (1996) 4780.
 - [9] A.A. de Laix, *Phys. Rev.* **D56** (1997) 6193.
 - [10] A.A. de Laix, L.M. Krauss and T. Vachaspati, *Phys. Rev. Lett.* **79** (1997) 1968.
 - [11] Y. Mellier *Annual Review of Astr. & Astrophys.* **37** (1999) 127.
 - [12] J.-P. Uzan and F. Bernardeau, *Cosmic String Lens Phenomenology: General Properties of Distortion Fields*, [[astro-ph/0004105](#)].
 - [13] P. Schneider, J. Ehlers and E.E. Falco, *Gravitational lenses* (Springer-Verlag, 1992).
 - [14] J.M. Bardeen, J.R. Bond, N. Kaiser and A.S. Szalay, *Astrophys. J.* **304** (1986) 15; J.R. Bond and G. Efstathiou, *Mon. Not. R. astr. Soc.* **226** (1987) 655.
 - [15] M. Hindmarsh, in *The formation and evolution of cosmic strings*, Eds. G.W. Gibbons, S.W. Hawking and T. Vachaspati, Cambridge University Press (1990) 527.

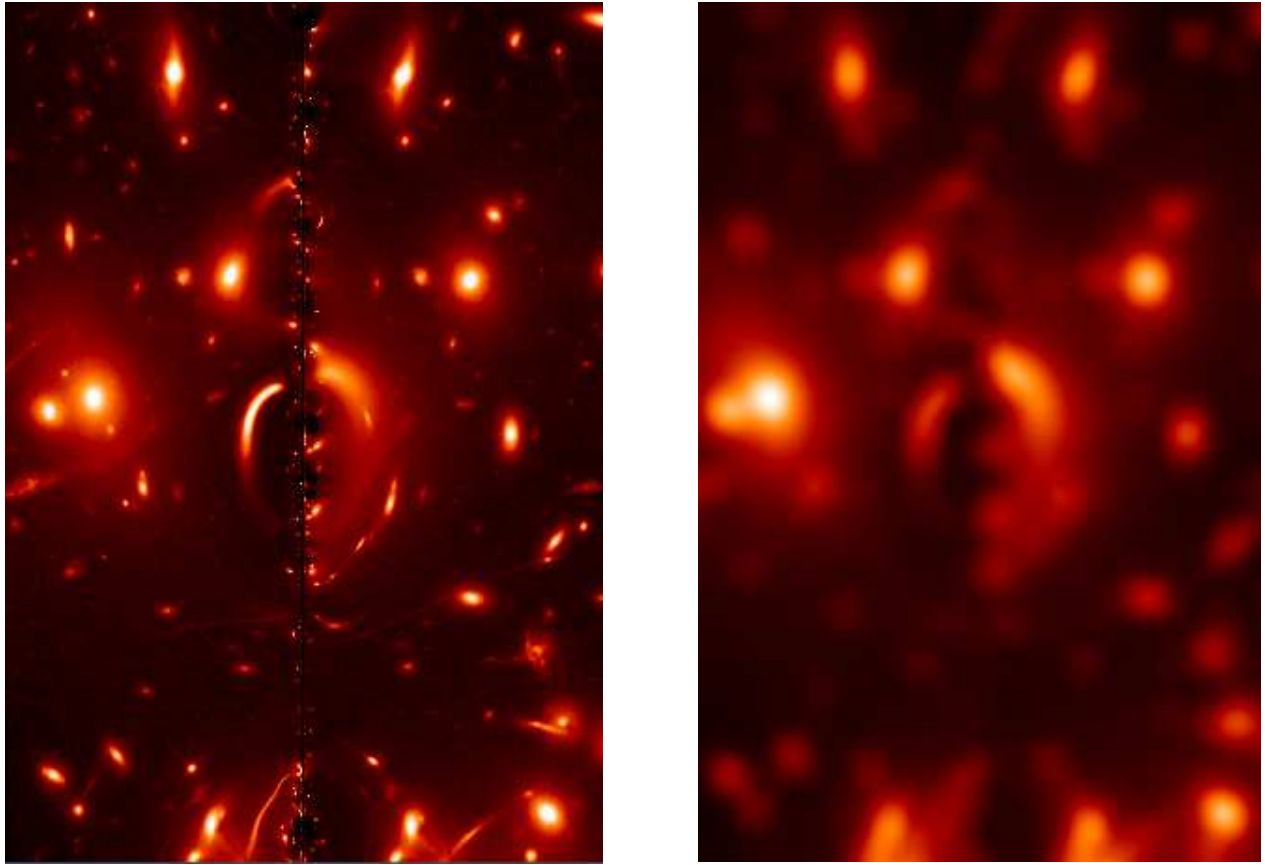


FIG. 4. Example of a deformed image by a Poisson string. The field corresponds to an external region of cluster A2218 (taken by the Hubble Space Telescope). If such a field was put at $z = 1$, then an intercepting string at $z \sim 0.8$ along the line-of-sight would produce multiple images as observed on the 2 pictures (the typical pair separation is about 5 arcsec). The right panel shows this system with a resolution of about 0.5 arcsec, whereas the left panel shows the same image with sub 0.1 arcsec resolution. In this case the distortions of the background galaxies are clearly exhibited. Note also that a number of small images appear along the string. In high resolution images, that might be the most effective way of detecting strings.